Articles

The 2.1-Å Resolution Structure of Iron Superoxide Dismutase from *Pseudomonas ovalis*[†,‡]

Barry L. Stoddard,*[,§] P. Lynne Howell,[‖] Dagmar Ringe,[§] and Gregory A. Petsko[§]
Department of Chemistry, Massachusetts Institute of Technology, Cambridge, Massachusetts 02139
Received February 15, 1990; Revised Manuscript Received June 18, 1990

ABSTRACT: The 2.1-Å resolution crystal structure of native uncomplexed iron superoxide dismutase (EC 1.15.1.1) from *Pseudomonas ovalis* was solved and refined to a final *R* factor of 24%. The dimeric structure contains one catalytic iron center per monomer with an asymmetric trigonal-bipyramidal coordination of protein ligands to the metal. Each monomer contains two domains, with the trigonal ligands (histidines 74 and 160; aspartate 156) contributed by the large domain and stabilized by an extended hydrogen-bonded network, including residues from opposing monomers. The axial ligand (histidine 26) is found on the small domain and does not participate extensively in the stabilizing H-bond network. The open axial coordination position of the iron is devoid of bound water molecules or anions. The metal is located 0.5 Å out of the plane of the trigonal ligands toward histidine 26, providing a slightly skewed coordination away from the iron binding site. The molecule contains a glutamine residue in the active site which is conserved between all iron enzymes sequenced to data but which is conserved among all manganese SODs at a separate position in the sequence. This residue shows the same structural interactions in both cases, implying that iron and manganese SODs are second-site revertants of one another.

Superoxide dismutase was first isolated and characterized from bovine erythrocytes by McCord and Fridovich in 1969 as a trace impurity of a carbonic anhydrase preparation and found to be capable of suppressing xanthine oxidase dependent univalent chemical reductions. They proposed the novel activity for the enzyme of dismuting the superoxide radical into oxygen and peroxide. This hypothesis led to a wide-ranging discussion in the literature concerning the effects of oxygen toxicity and the true catalytic nature of SOD (Fee, 1982; Halliwell, 1982). SOD is induced in a variety of mammalian tissue sources by exposure of the organism to hyperbaric oxygen, as well as in the cytoplasm of most, if not all, aerobic bacteria (Fridovich, 1975). Temperature-sensitive mutations of *Escherichia coli* SOD activity produce an organism with parallel defects in their tolerance for oxygen (McCord et al., 1973). The toxic, oxygen-dependent effects of species such as streptonigrin (Gregory & Fridovich, 1973) and paraquat (Autor, 1974) are reduced by the induction of superoxide dismutase activity. Recently, studies using *E. coli* SOD(−) double mutants have shown that such a strain is unable to grow on minimal media in the presence of oxygen and is highly sensitive to paraquat and to H_2O_2 (Carlioz & Touati, 1986). Growth can be restored by complementation with an SOD-producing plasmid. Therefore, it is believed that the total absence of SOD in *E. coli* creates a conditional sensitivity to oxygen.

There have been three basic varieties of SOD isolated and studied in the past 20 years: a Cu/Zn form found primarily in eukaryotic sources and evolutionarily unrelated Mn and Fe enzymes which are found in certain fungi, prokaryotes, mitochondria, and some species of blue-green algae (Keele et al., 1970; Vance et al., 1972; Lavelle et al., 1974; Weisiger et al., 1973; Lumsden & Hall, 1974).

Iron and manganese SODs from bacterial sources have been shown by several crystallographic studies (Table I) to be structural homologues. The iron protein has been reported to be constitutive under most growth conditions, whereas the manganese protein is induced in the presence of oxygen [an observation that does not appear to be dependent on the intracellular concentration of O_2^- (Nettleton et al. (1984)]. Production of the manganese-containing enzyme has been shown to be under the control of the SOD(a) gene and to proceed through a pro-Mn form of SOD which appears to be occupied by a foreign metal species and is totally inactive (Privalle et al., 1989). The active sites of the iron and manganese enzymes share completely conserved ligands and aromatic residues around the catalytic metal ions, including conserved tyrosines and tryptophans at a distance of up to 8 Å away from the catalytic metal. However, SODs from aerobic sources possess the interesting property of being absolutely specific for the metals they are normally associated with in terms of activity. For example, even though *Pseudomonas ovalis* apo-FeSOD has a very high natural affinity for Mn, Cd, and Cr, none of these replacements yields even slightly active enzyme (Yamakura & Suzuki, 1980). Similar experiments have given identical results for *E. coli* MnSOD (Ose & Fridovich, 1978). Even though the native enzymes show little or no differences in structure through X-ray crystallography, they show differences in solution for such properties as dimer integrity (Beyer et al., 1989), sensitivity to azide inhibition (Misra & Fridovich, 1978), and specific activity and inactivation by H_2O_2 (Beyer & Fridovich, 1986, 1987). Reports exist of SODs purified from anaerobic sources such as

[†] This work was supported in part by the Pittsburgh Supercomputer Facility through a grant of CPU time specifically for this project, as well as by Payload Systems, Inc., of Cambridge, MA. In addition, B.L.S. was supported as a Whitaker College Health Fund Fellow while this project was in process.

[‡] The coordinates for this structure have been deposited at the Brookhaven Protein Data Bank (Upton, Long Island, NY) with identifying code #1SDP, where they are available upon request.

* To whom correspondence should be addressed.
[§] Current address: Rosenstiel Basic Medical Sciences Research Center, Room 650, Brandeis University, Waltham, MA 02254.
[‖] Current address: Institute Pasteur, Paris, France.

0006-2960/90/0429-8885$02.50/0

Table I: Structures of Manganese- and Iron-Containing Superoxide Dismutase

source	metal	structure	resol (Å)	*R* factor (%)	ref
Th. thermophilus	Mn	tetramer	2.4		Stallings et al., 1985
B. stearothermophilus	Mn	dimer	2.4	26	Parker & Blake, 1988
E. coli	Fe	dimer	3.1		Carlioz et al., 1988
Ps. ovalis	Fe	dimer	2.1	24	Stoddard et al., 1990

Bacteroides fragilis (Gregory & Dapper, 1983) and *Propionibacterium shermanii* (Meier et al., 1982) which are reported to possess normal levels of activity with either metal incorporated into the active site, but to date none of these enzymes have been cloned or their genes sequenced.

The purpose of the present high-resolution structural studies of superoxide dismutase is to examine metal specificity among SODs and other similar metalloenzymes, as well as to provide structural data regarding the mechanism of action of radical-scavenging systems in the cell.

Materials and Methods

The crystallization, 2.9 Å resolution data collection, phase determination, and initial chain tracing have been described previously (Ringe et al., 1983). Briefly, single crystals of FeSOD were grown by batch methods from 55% saturated ammonium sulfate at pH 4.8 and 4 °C. The crystals are large orange rhombohedral plates, approximately 1 mm × 1 mm × 0.4 mm, prone to twinning along the B^* axis, and belong to space group $P2_1$, a = 81.9 Å, b = 49.1 Å, c = 61.7 Å, and β = 106.8°. The unit cell contains two asymmetric units, each composed of the enzyme dimer. For high-resolution data collection, crystals were mounted in quartz capillaries with a long edge parallel to the tube. The capillaries were sealed at both ends by mother liquor, mineral oil, wax, and Duco cement.

High-Resolution Data Collection. Crystallographic data were collected to 2.1-Å resolution at 4 °C on a Nicolet P3 diffractometer with two separate crystals, one for the 2.9–2.5-Å shell and a second for the data to 2.1 Å. Crystals were chosen which exhibit the least degree of twinning as shown by the average peak profile on ω for all three reciprocal axis directions. These data were scaled against and merged with the native 2.9-Å data set which was used for the original structural solution. For both crystals 450 low-resolution reflections were collected for scaling against the 2.9-Å native data set. A small overlap (750 reflections) was also collected between the two high-resolution crystals themselves. The 2.9–2.5-Å shell was collected by means of 1° ω scans with individual background measurements for each reflection in a manner similar to that for the 2.9-Å native data. The 2.1-Å shell was collected by step scans on ω (Wyckoff et al., 1967) with 11 steps of 0.03° each measured and the peak taken from the seven consecutive highest values. A background curve was measured with 96 points between 2θ = 2° and 2θ = 48°. Neither crystal suffered over 30% radiation damage during the course of data collection, and the total data collection time for each crystal was 73 and 64 h, respectively. Standard reflections were collected every 300 measurements to scale the data for radiation decay against time, and the linear correlation coefficient (Fletterick et al., 1976) was 0.96 for both shells. An absorbance curve was collected over a full 360° on φ with 24 separate 1° ω scans by use of individual background measurements for each point; the data were scaled over φ accordingly (North et al., 1968). The maximum absorption correction applied to the 2.5- and 2.1-Å data was 2.04 and 1.48, respectively. This strong absorbance effect is due to the irregular plate-like shape of the crystals. Friedel pairs were not collected. The overall *R* factor for scaling the three data sets together was 6% on *F*'s. A summary of all native data collection is presented in Table II.

Table II: Summary of Data Sets and Crystallographic Structure

data			
crystal	1	2	3
resolution shells (Å)	∞ to 2.9	2.9–2.5	2.5–2.1
Friedel *R* factor (on *F*) (%)	3	none	none
total radiation decay (%)	25	30	31
background correction	individual	individual	Wyckoff scans
R_{Merge} with crystal 1 (on *I*) (%)		8.6	12.2
R_{Merge} with crystal 2 (on *I*) (%)	8.6		11.8
average I/σ (*I*)	31.0	24.6	13.1
total reflections		21 140	
% of total data		72	
% by resolution	59 (∞ to 6 Å)	80 (6–3 Å)	70 (3–2.4 Å) 62 (2.1 Å)
structure			
non-hydrogen protein atoms	2912		
total water molecules	180		
initial overall *R* (%)[a]	49.7		
final overall *R* (%)	24.0		
bond distance RMS/σ[b]	0.026/0.030		
planar group RMS/σ	0.022/0.025		
chiral center RMS/σ	0.231/0.200		
nonbonded contact RMS/σ			
single torsion	0.242/0.500		
multiple torsion	0.280/0.500		

[a] $R = \sum(F_o - F_c)/\sum F_o$. [b] σ = restraint applied for deviation of refinement parameter(s) from ideality.

Fitting and Refinement of the Native Structure. Electron density averaging across the noncrystallographic 2-fold axis relating the two monomers was initially used to provide a clear map for building, and then each subunit was independently rebuilt into an unaveraged map of the dimer immediately before refinement was begun. The backbone was initially built into 2.9-Å minimaps as an α-carbon chain; this tracing was published previously (Ringe et al., 1983). This model was then converted into a polyalanine backbone with FRODO (Jones, 1978) on an Evans and Sutherland 300 color graphics system. At this point 180 residues out of 195 total in each monomer were accounted for. By use of the sequence for FeSOD published by Isobe et al. (1987), side chains were then built into the 2.9-Å map. With sequence data available, five more residues were built into the structure, leaving five residues unobserved at both the amino and carboxyl termini. These residues are unobservable in the electron density maps at all resolutions and refinement stages and are presumed disordered.

Initial refinement was performed at 2.9-Å resolution with restrained least squares (Prolsq). Three rounds of refinement, 15 cycles each, with intervening manual rebuilding against $3F_o - 2F_c$ Fourier difference maps were performed, driving the overall *R* factor for the 2.9-Å data from 49.7% to 29.2%. The maps used at this stage were calculated with the coordinates of up to 20 residues which were undergoing rebuilding deleted from the phase calculation to lower the intrinsic bias due to the model. Further least-squares refinement after these first three rounds yielded little improvement, leading us to refinement against the entire data set (10–2.1 Å) using the XPLOR molecular dynamics refinement method developed by Brunger et al. (1987). The initial *R* factor against the entire

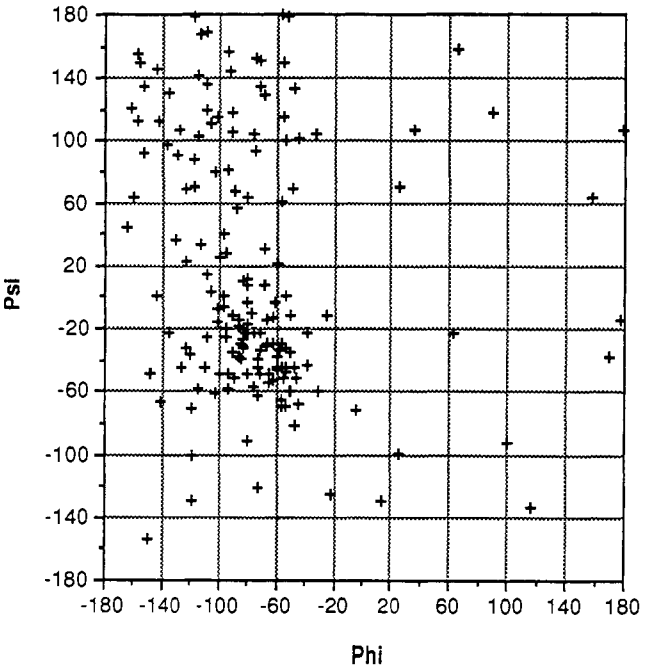

FIGURE 1: Ramachandran plot of the peptide torsion angles for individual residues of the enzyme monomer. The majority of residues fall in regions of right-handed α-helices and β-sheet.

data set to 2.1-Å resolution was 40%. We used a protocol in which the structure, after the initial static energy minimization, is heated to 4000 °C and then immediately placed into a slow-cooling (50 ps) annealing minimization. No extended dynamics were performed during the heat stage of the refinement. This stage of the refinement led to an initial decrease in the R factor from 40% to 34%, which seemed disappointingly high. The entire data set was then culled against intensity with the weakest 15% of the reflections being rejected (2300 out of 21 000 total reflections), and the refinement was repeated from scratch. This refinement produced a dramatic decrease in the R factor (from 40% to 26%) with the remaining data (18 811 independent structure factors). Difference maps were immediately calculated, and manual rebuilding was performed as before. At this stage 180 water molecules were built into the model. We were conservative in our use of water molecules after the dynamics refinement in order to avoid biasing toward a possibly incorrect structure. One final round of Prolsq against the entire unculled data set, using individual B factors for the first time, drove the R factor to its final value of 24.0% for 21 140 independent reflections between 50 and 2.1 Å. The Babinet correction for solvent scattering (Fraser et al., 1978) was used for low-resolution terms, with a small reduction of about 2% in the low-resolution (50–10 Å) R factors. Table II presents a summary of the refinements performed. There were 807 distances out of a total of 11 231 which deviated by greater than 0.06 Å from their ideal covalent bond distances. The R factor curve increases from a low of 23% for the 6–4-Å shell to an average of 26% for the higher resolution shells. The data are evenly and well represented to 2.1-Å resolution, with 80% of the predicted reflections between ∞ and 3.0 Å present in the final data set and 50% (1870 out of 3655 reflections) present in the highest resolution range (2.2–2.1 Å). Wilson plots[1] of the native data (from 10- to 2.1-Å resolution) yield an estimated overall B factor of 10.4

[1] $\ln [\mathrm{av}(I)/\sum(Fj^2)] = -2B \sin(2\theta/\lambda_2) + \ln K$. Therefore, a plot of $\ln [\mathrm{av}(I)/\sum(Fj^2)]$ vs $\sin^2(\theta/\lambda^2)$ gives a straight line with a slope of $-2B$, where B is the overall thermal factor for the resolution range used.

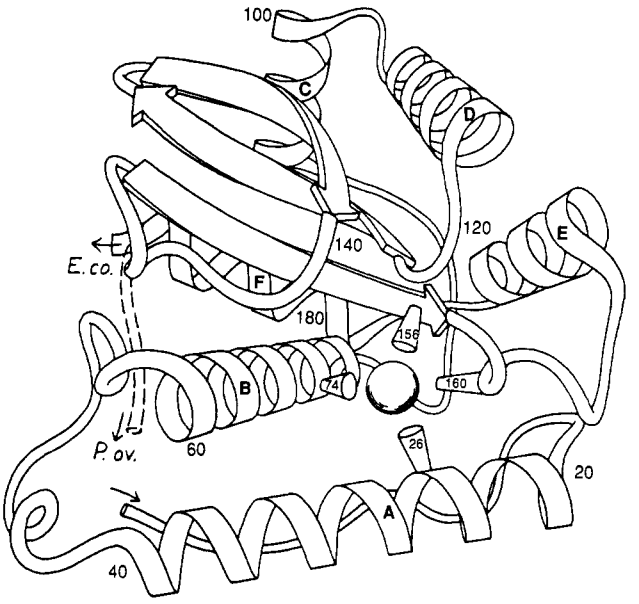

FIGURE 2: Iron and manganese superoxide dismutase fold. The various elements of secondary structure for the protein (helices A–F, antiparallel β-strands 1, 2, and 3) and the locations of the four ligands to the iron are shown, with histidine 26 as the bottom ligand. This figure is taken with permission from Ringe et al. (1983).

Å^2. Luzzati analysis of the refined structure provides an estimate of the mean coordinate error of 0.3 Å. The final ΔF maps of the structure reveal no significant peaks attributable to mistraced or incorrect coordinates. A plot of the peptide torsion angles φ and ψ for the individual residues of the enzyme monomer are shown in Figure 1.

RESULTS

Architecture of the Protein. The basic structure of the enzyme has been described in detail previously (Table I). In this paper we number the residues from the first monomer consecutively from 5 to 190 and from the second monomer from 205 to 390 in order to discuss interactions extending across the dimer interface. The enzyme monomer (Figure 2) consists of two domains. In this paper the domains are operationally defined as consisting of residues 1–40 (including helix A) and residues 60–190. The reasons for this are 2-fold: the large domain contributes three fixed, planar ligands to the iron in a trigonal arrangement which are stabilized by an extensive hydrogen-bonding network found solely within residues 60–190, while the small subunit contributes a distinct ligand to the iron which is orthogonal to the trigonal plane and relatively free from stabilizing hydrogen bonds. In addition, binding of inhibitor appears to cause conformational changes within the monomer centered about the specific movement of helix A relative to the rest of the protein, a movement that is facilitated by torsional rotations within the connecting loop of residues 40–60 (Stoddard et al., submitted for publication). Thus, the first domain contains a single five-turn α-helix and provides a single ligand (histidine 26) to the active site iron. The larger domain contains five helices surrounding a three-stranded antiparallel β-sheet and provides the three planar ligands (His 74 and 160; Asp 156) to the iron. The two domains are connected by a flexible 20-residue random coil (residues 40–50) which provides the necessary freedom for the two domains during catalysis, and the iron is found at the domain interface.

The stabilizing interactions observed for the separate regions of secondary structure are of a wide variety. Helix A is relatively well separated from the globular large domain and

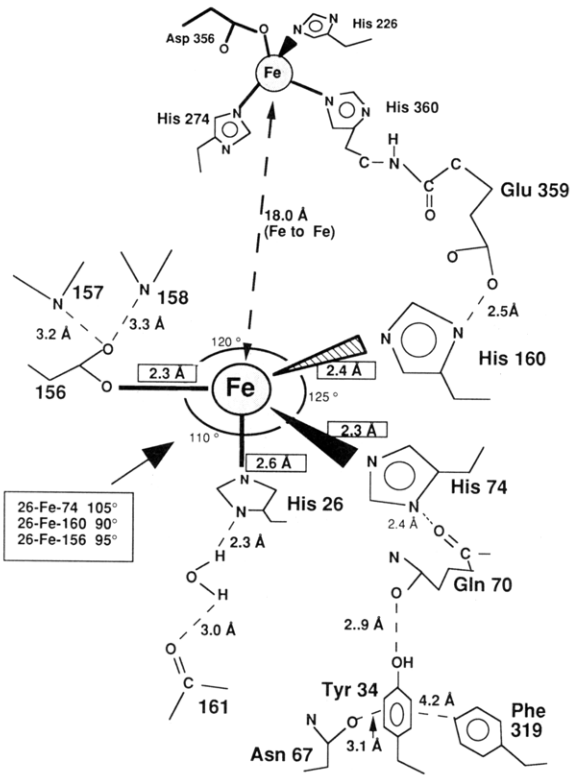

FIGURE 3: Geometry and coordination of iron ligands and hydrogen-bond network. The three planar ligands all possess strong polar interactions with the surrounding protein, while His 26 is hydrogen-bonded to a water molecule which forms a bridge to the protein backbone. Histidine 160 is bound by its δ-nitrogen to the side-chain carboxyl of Glu 359 from the opposite monomer, providing a direct 15-atom link between the two catalytic metals. The two irons are located 18 Å apart, and the stabilizing networks of each monomer, while extremely similar, are not identical.

is connected to the rest of the protein by extended peptide regions on either end. The helix possesses a number of internal stabilizing electrostatic interactions along its entire length, most notably Ser 19–Thr 22, Lys 20–Glu 24, His 27–His 31, and Asp 28–Asn 32. Also observed for helix A is a distinct kink, previously reported to be caused by a $C{=}O_n$ to $N{-}H_{n+5}$ hydrogen bond between the backbone atoms of His 26 and His 31.

Helix B (residues 60–82), on the other hand, spans the entire diameter of the protein interior and possesses mostly buried nonpolar residues: Ile 64, Phe 65, Ala 68, Ala 69, Val 71, Trp 72, Phe 76, Trp 78, and Leu 81. This helix also provides a histidine ligand (74) to the iron. The next two helices of the large domain (C and D, residues 90–114) lead into the β-sheet structure and are best described as an amphipathic two-helix bundle which lies on the exterior of the protein. This region is stabilized by a cluster of aromatic residues (Phe 101, 104, 107, and 111) contributed by both helices and buried in the interior of the molecule.

The β-sheet region (residues 123–156) consists mostly of relatively small, nonpolar residues such as alanine and valine, which possess a relatively high solvent accessibility. The sheet is anchored at both ends by residues that play important roles in the active site of the enzyme. A pair of tryptophans leading into the first strand (Trp 123 and 125) are located at the open binding site at the iron atom and are held in place by strong nonpolar and aromatic contacts. The final two ligands to the iron (Asp 156 and 160) and another well-placed active site tryptophan (Trp 158) are found at the end of the third strand. There is also a pair of interactions (aside from the usual bonds between backbone nitrogens and carbonyls of opposing peptides) that appears to help "tie" the sheet together: a 3-Å hydrogen bond between the γ-oxygen of threonine 138 and the backbone carboxyl group of Phe 119 and a second hydrogen bond from the γ-oxygen of threonine 154 to the sulfur of cysteine 80. This type of interaction, although rare, is well documented (Vinogradov & Linnell, 1971).

The final 20 residues are comprised of two helices (E and F) of approximately 10 residues each. Both helices are relatively inaccessible to solvent and are composed mostly of aromatic (Tyr 173; Phe 177 and 185; Trp 178 and 183) and nonpolar (Leu 174, 180, and 181; Val 186) residues which are buried in the protein interior. Helix E contains the only two arginine residues in the protein sequence (167 and 170); of these, Arg 167 is an important residue in the stabilization of the dimer, while Arg 170 is exposed to solvent.

The Metal Ligands. The iron is bound to four protein ligands as shown in Figure 3. The catalytic metal possesses a distorted trigonal-bipyramidal coordination, also described as a distorted tetrahedron, as shown previously by Calioz et al. (1988), Stallings et al. (1985), and Parker and Blake (1988). The coordination is asymmetric, with the three planar ligands being histidine 74, aspartate 156, and histidine 160. The fourth ligand, histidine 26, is found at a "pyramidal" coordination position. The iron is located 0.5 Å out of the plane formed by the trigonal ligands, toward histidine 26 and away from the "open" coordination position of the metal. The iron is approximately equidistant from the trigonal ligands, with an average measured bond distance equal to 2.3 Å (His 74), 2.3 Å (Asp 156), and 2.4 Å (His 160). The bond distance to histidine 26 is 2.6 Å.

The position of the metal out of the plane of the ligands by 0.5 Å shifts the trigonal-pyramidal geometry of the iron toward a tetrahedral geometry. The "orthogonal" bond angles through the iron are actually 105°, 90°, and 95° from His 26 NE2 through the iron to His 74, His 160, and Asp 156, respectively (measurements of bond angles precise to about 5°). The trigonal bond angles also deviate slightly from the expected value of 120°, occurring instead at approximately 120°, 110°, and 125° as shown in Figure 3. Thus, the coordination of the planar ligands to the catalytic iron is skewed toward the open position of the trigonal bipyramid. The electron density observed at the iron does not indicate the presence of bound water or sulfate.

The Ligand-Stabilizing Network. The trigonal ligands, which seem to be quite rigidly held in place about the metal, are in fact stabilized by an extensive hydrogen-bonding net-

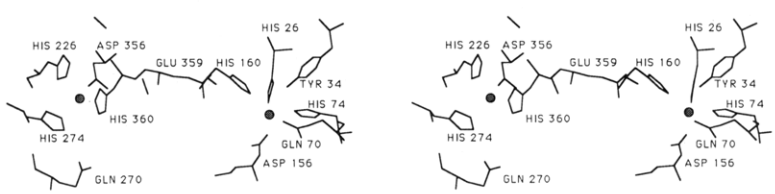

FIGURE 4: Stereoview of the ligand-stabilizing network connecting the two catalytic irons. Bonds are drawn between the metals and their ligands as well as between histidine 160 and glutamate 359.

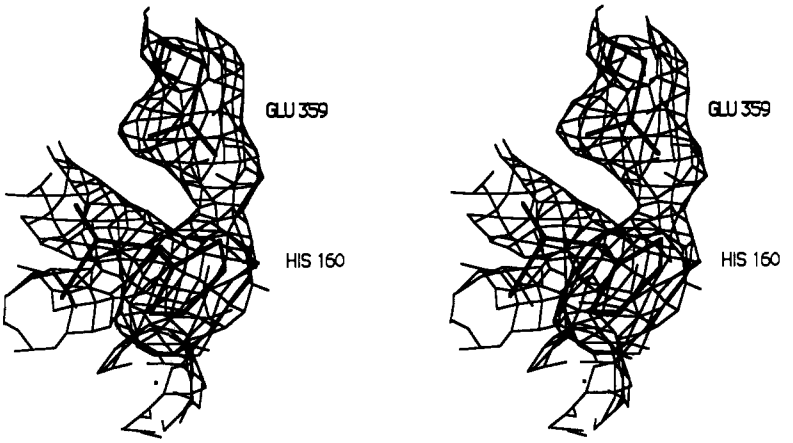

FIGURE 5: $2F_o - F_c$ delete map of the His 160–Glu 359 interaction which extends across the dimer interface and directly links the two active sites of the enzyme. Figure is contoured at 2σ.

work which spans the dimer interface (Figure 4). The free carboxyl oxygen of Asp 156 is bound to amino nitrogens 157 and 158 of the protein backbone with oxygen to nitrogen distances of 3.2 and 3.3 Å, respectively. Histidine 74 has a very tight electrostatic interaction (2.4 Å) with the main-chain carboxyl oxygen of glutamine 70. The side chain of Gln 70 is hydrogen bonded to the phenolic oxygen of the strictly conserved tyrosine 34 (bond length = 2.9 Å) and is found in close proximity to tryptophan 123, one of two conserved indole rings observed to flank the substrate binding site in the enzyme. Tyrosine 34 is further stabilized by weakly polar interactions with Phe 319 (from the second protein subunit) and the side chain of Asn 67. The bond angle from Tyr 34 CZ through the phenyl oxygen to the glutamine side chain is approximately 130°, which is reasonable for an interaction involving the proton of an sp^3 phenolic oxygen. The interaction between glutamine and tyrosine 34 in the active site is structurally conserved throughout all manganese and iron SODs; however, the position of this glutamine in the protein sequence is quite different between these two varieties of the enzyme (Figure 8), a difference in conservation which may play a role in the specificity of the enzyme for a given metal cofactor.

The δ-nitrogen of histidine 160 is also engaged in a tight electrostatic interaction (2.5 Å) with the charged side chain of Glu 359 (from the second subunit), a bond which provides a direct 15-atom bridge between the iron atoms of the monomers (Figure 5). The two irons themselves are found 17.9 Å from one another, and the two active sites display a high degree of folding cooperativity as described above. The Glu–His interaction is unambiguous in all initial maps and subsequent omit maps during refinement; the final refined distance is shorter than should be expected for a similar model hydrogen bond (2.6–2.8 Å) and is shorter than that reported for the same interaction in the *Thermus thermophilus* Mn-SOD structure (2.9 Å). This anomaly is due to the quality of the data used in these studies (see Discussion) and to the restraints applied to such noncovalent contact distances during refinement (Table II). However, the bond distance for this interaction is within the estimated error for atomic coordinates (0.3 Å) and noncovalent bond distances (0.5 Å) calculated for the refined structure by Luzzati analysis.

Histidine 26, which appears to possess a higher degree of mobility than its trigonal counterparts, is also stabilized by a hydrogen bond to its δ-nitrogen, but this 2.3-Å bond is to a water molecule, which in turn forms a bridge to the backbone carboxyl of alanine 161. Thus, the stabilizing network of interactions between ligands and the rest of the protein structure appears to provide a degree of rigidity to the planar

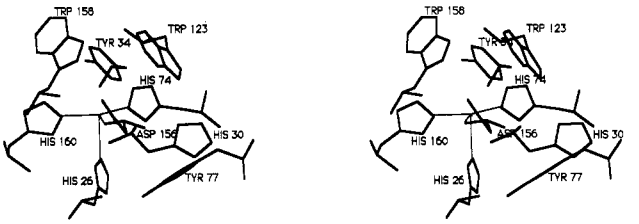

FIGURE 6: Stereoview of the aromatic residues found within an 8-Å sphere of the catalytic metal. Trp 123, Trp 158, and Tyr 34 are all found at the open coordination position of the iron atom and are assumed to play a role in the specificity and mechanism of the enzyme.

ligands but allows the histidine 26 to enjoy a certain amount of positional freedom.

The hydrogen-bonding network described above is duplicated in the second subunit of the dimer.

The Aromatic Active Site. One of the most interesting features of the iron and manganese SODs is the high, conserved aromatic content of the protein, especially in the area in close proximity to the active site. Thirty-three residues or 17% of the entire protein sequence, are His, Tyr, Phe, or Trp. Within an 8-Å sphere of the active site iron (Figure 6) are found five conserved aromatic residues in addition to the histidine ligands—tyrosine 34 and 77 (5.2 and 6.6 Å), histidine 30 (7.8 Å), and tryptophan 123 and 158 (5.5 and 4.5 Å). The tryptophan pair and tyrosine 34 are all found to border the open coordination position of the metal and may play important roles in the mechanism and specificity of the enzyme (see Discussion).

Dimer Stabilization. FeSOD from *Pseudomonas* is active only as a dimer (Figure 7), the characteristics of which appear to differ from that of dimeric MnSOD (Beier et al. 1989). Examination of the dimer interface shows 14 obvious electrostatic or polar interactions which serve specifically to stabilize the dimer interface. Of these bonds, which are detailed in Table III, seven (or about half) are weakly polar aromatic–aromatic interactions in which the partially negative π electron cloud of a phenyl ring face stacks against the edge of a second electron-poor ring edge as described earlier. An example of such a bond at the dimer interface is the 3.2-Å contact between tyrosine 25 of the first monomer and tyrosine 366 of the second, a contact that is estimated to be worth about 1–2 kcal/mol (Burley & Petsko, 1986).

The remaining dimer contacts are strong electrostatic and hydrogen-bond interactions, such as the 2.6-Å H-bond from glutamate 21 to the tyrosine 366 phenolic oxygen of the opposite monomer and the 2.5-Å serine 21 to serine 321 hydrogen bond between the monomers. Arginine 167 and 367 are both

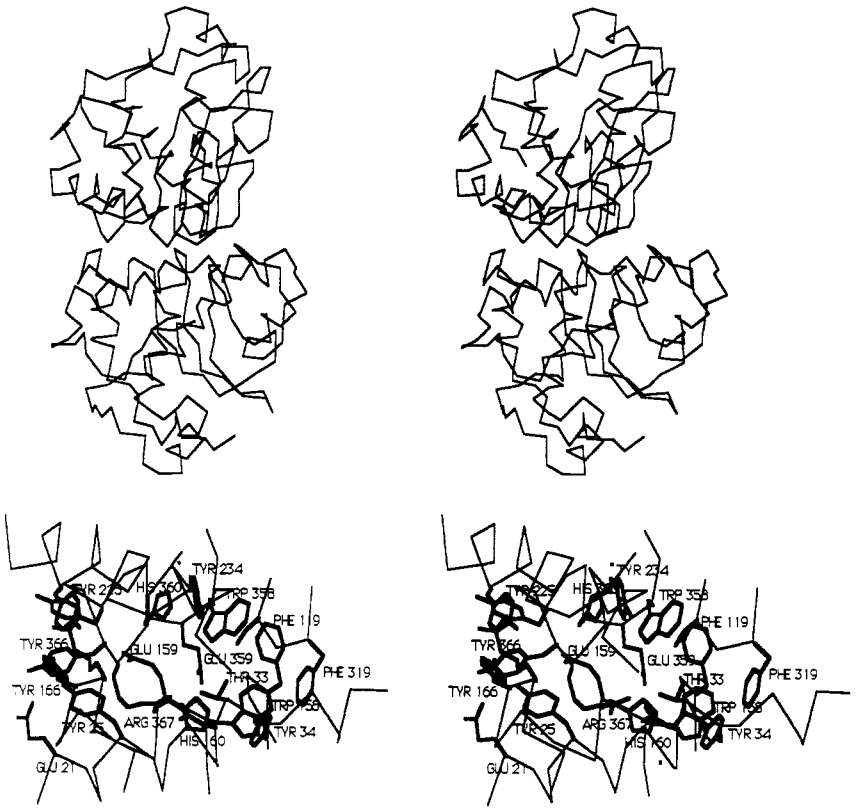

FIGURE 7: Stereoview of the dimer fold. The lower view is a view of the individual residues found to participate in dimer stabilization as summarized in Table III.

Table III: Dimer Stabilizing Interactions

monomer 1	monomer 2	bond	symmetric?
Glu 21	Tyr 366	Glu OE1 to Tyr OH, 2.6 Å	no
Tyr 25	Tyr 366	ring plane to ring edge, 3.3 Å	no
Asn 32	Arg 367	Asn OD2 to Arg NH1, 2.9 Å	no
Thr 33	Arg 367	Thr OG1 to Arg NH1, 2.9 Å	no
Tyr 34	Phe 319	ring plane to ring edge, 4.2 Å	yes
Phe 119	Tyr 234	ring plane to ring edge, 3.4 Å	yes
Phe 119	Trp 358	ring plane to rin edge, 3.2 Å	yes
Ser 121	Ser 321	Ser OG1 to Ser OG1, 2.5 Å	yes
Trp 158	Phe 319	ring plane to ring edge, 3.5 Å	yes
Glu 159	His 360	Glu OE1 to His ND1, 2.6 Å	yes
His 160	Glu 359	His ND1 to Glu OE2, 2.5 Å	yes
Tyr 166	Tyr 363	ring plane to ring edge, 3.2 Å	no
Tyr 166	Tyr 366	ring plane to ring edge, 3.4 Å	yes
Arg 167	Tyr 225	Arg NH to Tyr backbone C=O, 2.6 Å	no

involved in dimer stabilization, in one case forming a 2.9-Å bond to asparagine 32 and in the opposite direction making a 2.6-Å electrostatic contact with the backbone carboxyl of tyrosine 225. The most interesting bond from the standpoint of the active site, as discussed earlier, is the 2.5-Å hydrogen bond between the δ-nitrogen of the iron ligand histidine 160 and glutamate 359.

Of the 14 dimer contacts outlined in Table III, 8 are "symmetric" in that they occur identically in both directions; of these, two are contacts between the same residues of opposing monomers (a hydrogen bond from serine 121 and 321 and an aromatic interaction between tyrosine 166 and 366). Of the remaining eight "nonsymmetric" bonds, three involve residues that participate in dimer stabilization in one direction only (Glu 21, Asp 32, and Thr 33), while the rest involve residues that make different types of contacts in opposite directions; for example, tyrosine 25 makes contact with tyrosine 366 in one direction but is involved in a backbone hydrogen bond to Arg 167 NH1 in the opposite direction.

Discussion

This work reports the 2.1-Å refined structure of iron superoxide dismutase, an enzyme that binds and dismutes the reactive superoxide anion, O_2^-. Compared to values often obtained for many refined protein crystal structures, an R of 0.24 is high. Several comments on this point are warranted. FeSOD presents a host of intractable difficulties for crystallographic studies. Native iron dismutase crystals decay extremely rapidly in the X-ray beam (presumably due to the catalytic formation of peroxide from radiation-produced radical species during data collection). More importantly, FeSOD crystals from *Ps. ovalis* are always twinned to some extent (Ringe et al., 1983), and although twinning effects were taken into account in data collection and processing, a residual error certainly remains. Finally, it is known that "native" FeSOD crystals are actually mixtures of holo- and apoenzyme in a ratio of about 50:50. All attempts to add iron back to the crystals have failed, and although the high quality of the original MIR map in the region of the active site suggests that the two structures are virually identical, one cannot rule out the possibility that small differences exist and that we are trying to fit a single structural model to a data set that actually incorporates contributions from two slightly different structures. The variable occupancy of the metal site is accounted for in the individual B factors refined for the iron atoms as well as for the rest of the protein.

For all of these reasons, the data used in refinement of the FeSOD structure are not of optimal quality, and the R factor in an honest refinement should reflect this fact. However, we believe that the structure is correct both in overall terms and in detail and that there is strong internal and external evidence to support that belief. All final ΔF and omit maps are consistent with the model presented here. There is no significant

unexplained density in either subunit. The agreement between the two subunits, refined without any imposed noncrystallographic symmetry, is excellent. Possible alternative chain tracings have been explored extensively both in manual rebuilding and in additional rounds of simulated annealing refinement (XPLOR). Most importantly, the structure agrees both overall and in detail—especially in the region of the active site—with the independently determined structure of MnSOD (Table I), which was not used in any way in the building or refinement of this structure.

The structure and function of this protein raises a number of interesting questions about the specificity of the enzyme toward substrate and toward the metal cofactor which is required for catalysis. The most fundamental question regarding this enzyme is why this enzyme catalyzes the dismutation of superoxide, as opposed to any other metabolic process involving oxygen, such as the noncatalytic binding and release of O_2 exhibited by the globins.

Iron superoxide dismutase has some interesting correlations with the oxygen binding proteins myoglobin and hemoglobin. The three-dimensional folds of these proteins are quite different; however, the environments provided for the iron atoms are similar in several ways. The iron atom of SOD is bound with a trigonal planar array of protein ligands and is also bound to histidine 26, which is found orthogonal to the plane of the trigonal ligands. The iron atom is located approximately 0.5 Å out of the plane formed by these residues and is found on the same side of the protein plane as the histidine. The iron posses an open coordination site opposite His 26 for binding of substrate or inhibitor; the binding pocket is tightly flanked by a pair of tryptophan residues (123 and 158) which appear to be capable of preventing binding of nonlinear anions (phosphate, sulfate, carbonate, etc.) to the positively charge iron. Access to the binding site of SOD is rather limited and probably involves the movement of local portions of secondary structure. The two active sites appear to exhibit a great deal of cooperativity both in proper folding and stabilization of the structure and in activity of the enzyme (active monomeric FeSOD has never been isolated).

Myoglobin and hemoglobin also bind iron to a group of planar ligands, although the ligands in this case are the four nitrogen atoms of the porphyrin ring, so that the iron atom possesses s square-planar bipyramidal geometry with an absolutely symmetrical distribution of ligands within the plane of the metal. The iron is bound by a "proximal" histidine (His 93 for sperm whale) orthogonal to the porphyrin with a bond distance of 2.2 Å, and the metal is found approximately 0.4 Å out of the heme plane toward His 93 in the deoxy state. The iron contains an open binding position which is flanked by the ring of histidine 64, a residue that plays an important role in lowering the binding affinity of such species as carbon monoxide by virtue of steric hindrance (Kuriyan et al., 1986). As with FeSOD, accessibility to the oxygen binding pocket is rather limited and has been shown to involve the movement of several residues, including the distal histidine 64, arginine 45, and valine 68 (Ringe et al., 1984).

In spite of these mild similarities, the two proteins possess separate, distinct functions in the pathways of oxygen metabolism: the globins are responsible for the environmentally dependent binding and release of O_2 (and CO_2), whereas SOD binds reduced, anionic species of oxygen (specifically O_2^- and HO_2^-) as well as small anions such as azide and fluoride. The specificity of SOD toward anionic forms of oxygen can be ascribed to the coordination, valence, and electropotential of the catalytic iron and to the influence of protein residues proximal to the binding site. The first two of the iron parameters have been described by various investigators as detailed in the introduction; the third has been studied by Barrette et al. (1983), who report a redox potential for the reduction of ferric SOD from three sources of enzyme (including *Ps. ovalis*) at physiological pH equal to +0.26 V (as opposed to a standard E_0 of 0.77 V for the reduction of Fe^{3+}). As for the involvement of the protein in binding O_2^-, studies have shown that electrostatic interactions between substrate and positively charged side chains near the active site are an important factor in the catalyzed process, presumably through the facilitation of precollision orientation and directed diffusion of substrate (Benovic et al., 1983). Examination of the active site of FeSOD shows several candidate residues for such a role in catalysis close to the binding site channel, including lysine 29 and histidine 31 of helix A, lysine 51 in the flexible loop region connecting the two domains, asparagine 66 and 67 of helix B, and glutamine 70. Of these residues, Lys 29, His 31, and Asn 67 are completely conserved among all Mn and Fe SODs, while Lys 51, Asn 66, and Gln 70 are strictly conserved among all iron-containing dismutases but not conserved by manganese enzymes (Figure 8). Glutamine 70 is found closest to the binding pocket, participating in the ligand hydrogen-bonding network as shown in Figure 3.

Tyrosine 34 exhibits a strong polar interaction with glutamine 70 and is strictly conserved among all SODs. This residue, which is located at the substrate binding pocket, is found approximately 5 Å from the iron atom at the hydroxyl oxygen. It is likely that this tyrosine plays an important role in catalysis, through one of two possibilities:

(1) Acid/base catalysis, presumably by abstraction of a proton from solvent [known to be the rate-limiting step for this enzyme (Bannister et al., 1987)] and either the direct protonation of peroxide product or participation in a proton-transfer mechanism with a second residue. The tyrosine is in close enough proximity to the catalytic iron (5 Å) to play such a role. The importance of glutamine 70 in catalysis in conjunction with tyrosine 34 is strongly implied by the structural conservation of the residue at a different position in the sequence for all manganese SODs as discussed below.

(2) Participation in catalysis through the formation of a tyrosine radical. The possibility of tyrosine participating in catalysis through the generation of a hydroxyl radical which is then capable of single-electron transfer has been shown conclusively for ribonucleotide reductase from *E. coli* (Ashley & Stubbe, 1985). It is possible that tyrosine acts in conjunction with the metal ion to catalyze the dismutation of superoxide through a more complex mechanism than has been previously thought. A nonstandard mechanism would be consistent with the observation that very few other iron- or manganese-containing proteins or small molecules show significant dismutase activity (Halliwell, 1982). To this point, however, no evidence has been shown that supports the notion of a tyrosine radical involvement in the mechanism of SOD.

The most interesting feature of the prokaryotic SODs is the specificity of the enzymes for either iron or manganese. Every structural study to data has discussed the fact that, even though the active sites of Mn- and Fe-containing SOD are virtually identical in terms of sequence homology and structure, the enzymes from aerobic sources require the "correct" metal for catalysis to occur. Examination of the sequence of iron and manganese enzymes (Figure 8) shows a number of residues which are strictly conserved between enzymes with the same metal, but uniquely different between the two classes. One of these, Gln 70 (Fe)/Gly 70 (Mn), was mentioned earlier as

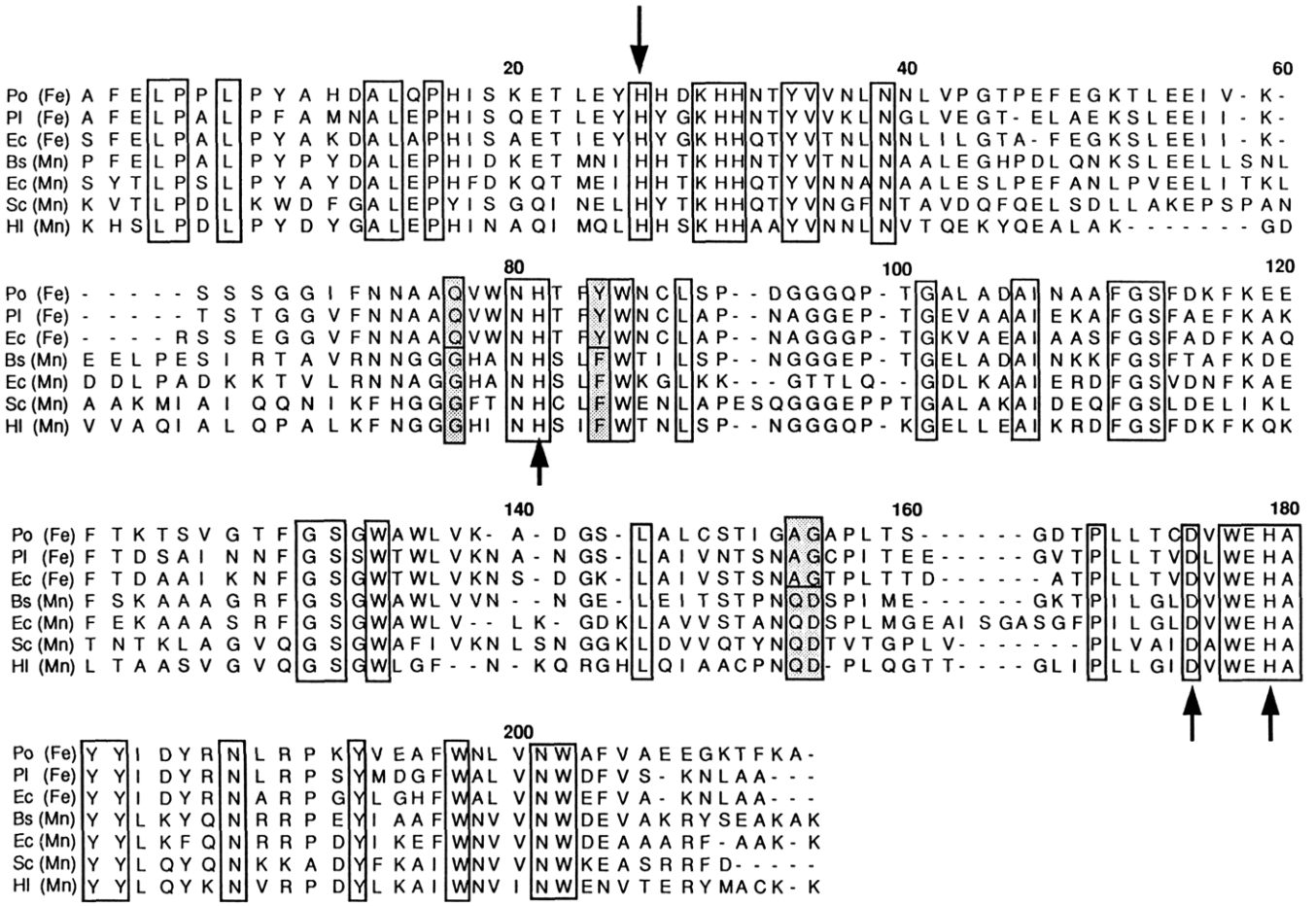

FIGURE 8: Protein sequences of three iron-containing and four manganese-containing SODs. The sources of enzyme are *E. coli* (Ec), *Ps. ovalis* (Po), *Photobacterium leiognathi* (Pl), *B. stearothermophilus* (Bs), yeast (Sc), and human liver (Hl). The four metal ligands are indicated by arrows. Completely conserved residues are indicated by clear boxes, while residues which are conserved among enzymes containing the same metal but different between the two separate classes of SOD are indicated by shaded boxes. Note the separate site conservation of the active site glutamine between the iron and manganese enzymes (position 70 for Fe, 154 for Mn).

the most obvious difference close to the active site metal. Interestingly, glutamine 141 in the manganese enzyme from *Bacillus stearothermophilus* has been shown to be conserved among all Mn-containing SODs and is bound to the conserved tyrosine 34 (in a manner identical with that of glutamine 70 in the iron enzyme), implying that the residue is important for either catalysis or structural stability and therefore has been conserved at a second site between the two families of SOD. This pattern of structural conservation was noted by Carlioz et al. (1988), and the glutamine was assigned a purely structural role. We believed this residue plays an important chemical, structural, or dynamic role in catalysis and may contribute to the metal specificity of the enzyme. These possibilities are discussed further in a separate paper.

What is clear, however, is that if the two forms of the enzyme do operate according to identical catalytic mechanisms, then the specificity observed toward their respective metal cofactors is difficult to explain on the basis of their similar structures. It is possible that the two related enzyme species have evolved similar but separate mechanisms for dismutation of superoxide that involve residues which differ between the two enzymes, as described above. According to such a scenario, the metal would play a critical and unique role in the catalytic mechanism employed by each enzyme, such that exchange of one metal for the other would have a deleterious effect on activity. The SODs appear to function by placing a metal redox center in a distinctly polar and yet hydrophobic environment quite unlike the normal medium where a species such as Fe^{3+} would normally be found; subtle differences in the metal environment matrix between the two enzymes are possibly very important in maintaining activity with specific metal cofactors.

ACKNOWLEDGMENTS

We acknowledge the help and advice of Dr. Rob Campbell, Dr. Greg Farber, and Dr. Steven C. Almo on this project.

Registry No. SOD, 9054-89-1; Fe, 7439-89-6.

REFERENCES

Ashley, G. W., & Stubbe, J. (1985) *Pharmacol. Ther. 30*, 301–329.

Autor, A. P. (1974) *Life Sci. 14*, 1309–1319.

Barrette, W. C., Sawyer, D. T., Fee, J. A., & Asada, K. (1983) *Biochemistry 22*, 624–627.

Beier, W. F., & Fridovich, I. (1986) in *Manganese in Metabolism and Enzyme Function* (Schramm, V. L., & Wedler, F. C., Eds.) p 193, Academic Press, New York.

Beier, W. F., & Fridovich, I. (1987) *Biochemistry 26*, 1251.

Beier, W. F., Reynolds, J. A., & Fridovich, I. (1989) *Biochemistry 28*, 4403–4409.

Benovic, J., Tillman, T., Cudd, A., & Fridovich, I. (1983) *Arch. Biochem. Biophys. 221*, 329–332.

Brunger, A. T., Kuriyan, J., & Karplus, M. (1987) *Science 235*, 458–460.

Burley, S. K., & Petsko, G. A. (1986) *J. Am. Chem. Soc. 108*, 7995.

Burley, S. K., & Petsko, G. A. (1988) *Adv. Protein Chem. 39*, 125–189.
Carlioz, A., & Touati, D. (1986) *EMBO J. 5*, 623–630.
Carlioz, A., Ludwig, M. L., Stallings, W. C., Fee, J. A., Steinman, H. M., & Touati, D. (1988) *J. Biol. Chem. 263*, 1555–1562.
Fee, J. A. (1982) *Trends Biochem. Sci. 7*, 84–86.
Fletterick, J., et al. (1976) *J. Mol. Biol. 103*, 1–13.
Fraser, R. D. B., MacRae, T. P., & Suzuki, E. (1978) *J. Appl. Crystallogr. 11*, 693–694.
Fridovich, I. (1972) in *Horizons in Biochemistry and Biophysics* (Quaglierello, E., Ed.) Vol. 1, p 1, Addison-Wesley, Reading, MA.
Fridovich, I. (1975) *Annu. Rev. Biochem. 44*, 147–158.
Gregory, E. M., & Dapper, C. H. (1983) *Arch. Biochem. Biophys. 220*, 293–300.
Gregory, E. M., Goscin, S. A., & Fridovich, I. (1973) *J. Bacteriol. 114*, 1193–1197.
Halliwell, B. (1982) *Trends Biochem. Sci. 7*, 270–272.
Isobe, T., Fang, Y., Muno, D., Okuyama, T., Ohmori, D., & Yamakura, F. (1987) *FEBS Lett. 223*, 92–96.
Jones, T. A. (1978) *J. Appl. Crystallogr. 11*, 268–272.
Keele, B. B., Jr., McCord, J. M., & Fridovich, I. (1970) *J. Biol. Chem. 245*, 6176–6181.
Kuryan, J., Wilz, S., Karplus, M., & Petsko, G. A. (1986) *J. Mol. Biol. 192*, 133–154.
Lavelle, F., Durosay, P., & Michelson, A. A. (1974) *Biochimie 56*, 451–458.
Lumsden, J., & Hall, D. O. (1974) *Biochem. Biophys. Res. Commun. 58*, 35–41.
McCord, J. M., & Fridovich, I. (1969) *J. Biol. Chem. 244*, 6049–6055.
McCord, J. M., Beauchamp, C. O., Goscin, S., Misra, H. P., & Fridovich, I. (1973) *Oxidases and Related Redox Systems*, Vol. 51, p 76, University Park Press, Balitmore, MD.
Meier, B., Barra, D., Bossa, I. F., Calabrese, L., & Rotilio, G. (1982) *J. Biol. Chem. 257*, 13977.
Misra, H. P., & Fridovich, I. (1978) *Arch. Biochem. Biophys. 189*, 317.
Nettleton, C. J., Bull, C., Baldwin, T. O., & Fee, J. A. (1984) *Proc. Natl. Acad. Sci. U.S.A. 81*, 4970–4973.
North, A. C. T., Phillips, D. C., & Mathews, F. S. (1968) *Acta Crystallogr. A24*, 351–359.
Ose, D. E., & Fridovich, I. (1979) *Arch. Biochem. Biophys. 194*, 360–364.
Parker, M. W., & Blake, C. C. F. (1988) *J. Mol. Biol. 199*, 649–661.
Privalle, C., Beyer, W. F., & Fridovich, I. (1989) *J. Biol. Chem. 264*, 2758–2763.
Ringe, D., Petsko, G. A., Yamakura, F., Suzuki, K., & Ohmori, D. (1983) *Proc. Natl. Acad. Sci. U.S.A. 80*, 3879–3883.
Ringe, D., Petsko, G. A., Kerr, D. E., & Ortiz de Montellano, P. R. (1984) *Biochemistry 23*, 2–4.
Stallings, W. C., Pattridge, K. A., Strong, R. K., & Ludwig, M. L. (1985) *J. Biol. Chem. 260*, 16424–16432.
Sundaralingam, M., Drendel, W., & Greaser, M. (1985) *Proc. Natl. Acad. Sci. U.S.A. 82*, 7944–7947.
Vance, P. G., Keele, B. B., Jr., & Rajagopalan, K. V. (1972) *J. Biol. Chem. 247*, 4782–4786.
Vinogradov, S. N., & Linnell, R. H. (1971) *Hydrogen Bonding*, Van Nostrand Reinhold, New York.
Weisiger, R. A., & Fridovich, I. (1973) *J. Biol. Chem. 248*, 4793–4796.
Wyckoff, H. W., Doscher, M. S., Tsernoglou, D., Inagami, T., Johnson, D., & Richards, F. M. (1967) *J. Mol. Biol. 27*, 563.
Yamakura, F., & Suzuki, K. (1980) *J. Biochem. 88*, 191–196.